HHS Public Access

Author manuscript

Glia. Author manuscript; available in PMC 2021 April 01.

Published in final edited form as:

Glia. 2020 October ; 68(10): 1987–2000. doi:10.1002/glia.23817.

Tanycyte ablation in the arcuate nucleus and median eminence increases obesity susceptibility by increasing body fat content in male mice

Sooyeon Yoo[1], **David Cha**[1], **Soohyun Kim**[2], **Lizhi Jiang**[1], **Patrick Cooke**[1], **Mobolanie Adebesin**[1], **Andrew Wolfe**[3], **Ryan Riddle**[2,4], **Susan Aja**[1], **Seth Blackshaw**[1,5,6,7,8]

[1]Solomon H. Snyder Department of Neuroscience, Johns Hopkins University School of Medicine, Baltimore, Maryland [2]Department of Orthopedic Surgery, Johns Hopkins University School of Medicine, Baltimore, Maryland [3]Department of Pediatrics, Johns Hopkins University School of Medicine, Baltimore, Maryland [4]Baltimore Veterans Administration Medical Center, Baltimore, Maryland [5]Department of Ophthalmology, Johns Hopkins University School of Medicine, Baltimore, Maryland [6]Department of Neurology, Johns Hopkins University School of Medicine, Baltimore, Maryland [7]Center for Human Systems Biology, Johns Hopkins University School of Medicine, Baltimore, Maryland [8]Institute for Cell Engineering, Johns Hopkins University School of Medicine, Baltimore, Maryland

Abstract

Tanycytes are radial glial cells located in the mediobasal hypothalamus. Recent studies have proposed that tanycytes play an important role in hypothalamic control of energy homeostasis, although this has not been directly tested. Here, we report the phenotype of mice in which tanycytes of the arcuate nucleus and median eminence were conditionally ablated in adult mice. Although the cerebrospinal fluid-hypothalamic barrier was rendered more permeable following tanycyte ablation, neither the blood-hypothalamic barrier nor leptin-induced pSTAT3 activation in hypothalamic parenchyma were affected. We observed a significant increase in visceral fat distribution accompanying insulin insensitivity in male mice, without significant effect on either body weight or food intake. A high-fat diet tended to accelerate overall body weight gain in tanycyte-ablated mice, but the development of visceral adiposity and insulin insensitivity was comparable to wildtype. Thermoneutral housing exacerbated fat accumulation and produced a shift away from fat oxidation in tanycyte-ablated mice. These results clarify the extent to which tanycytes regulate energy balance, and demonstrate a role for tanycytes in regulating fat metabolism.

Correspondence: Seth Blackshaw, Solomon H. Snyder Department of Neuroscience, Johns Hopkins University School of Medicine, Baltimore, MD. sblack@jhmi.edu.

Conflict Of Interest

The authors declare no competing financial interests.

Data Availability Statement

This manuscript has been deposited in bioRxiv (doi: https://doi.org/10.1101/637587). The authors declare that all data supporting the findings of this study are available within the paper and its Supporting Information files.

Supporting Information

Additional supporting information may be found online in the Supporting Information section at the end of this article.

Keywords

adipose; blood–brain barrier; energy homeostasis; hypothalamus; insulin insensitivity; metabolism; radial glia; tanycytes; thyroid

1 | Introduction

Tanycytes are radial glia that line the ventricular wall of the mediobasal hypothalamus. These are divided into alpha- and beta-sub-types, based on their dorsoventral position along the third ventricle.They extend elongated foot processes away from the ventricle, which terminate either on blood vessels in the hypothalamic parenchyma or at the ventral pial surface (E. Rodríguez, Guerra, Peruzzo, & Blázquez, 2019). Beta-tanycytes reside outside the blood–brain barrier, and directly contact fenestrated capillaries in the median eminence (E. M. Rodríguez, Blázquez, & Guerra, 2010). Their location at the interface between the hypothalamus and circulatory system allows tanycytes to regulate a broad range of processes relevant to hypothalamic physiology. These include control of the blood-hypothalamus barrier (Langlet et al., 2013; Mullier, Bouret, Prevot, & Dehouck, 2010), energy and nutrient sensing (Ebling & Lewis, 2018; R. Elizondo-Vega et al., 2015; R. J. Elizondo-Vega, Recabal, & Oyarce, 2019), and regulation of neurohormone release (Müller-Fielitz et al., 2017; Parkash et al., 2015). Tanycytes also express many markers of neural progenitor cells, and have been reported to show limited neurogenic potential (Haan et al., 2013; Lee et al., 2012; Yoo & Blackshaw, 2018).

Recently, there has been growing interest in the potential role of tanycytes in regulating energy metabolism (Ebling & Lewis, 2018; García-Cáceres et al., 2019; Prevot et al., 2018). Tanycytes have been reported to directly sense glucose and amino acid levels in cerebrospinal fluid (CSF) and blood (Benford et al., 2017; Frayling, Britton, & Dale, 2011; Lazutkaite, Soldà, Lossow, Meyerhof, & Dale, 2017), to actively transport leptin into the hypothalamus (Balland et al., 2014), and to regulate production and release of thyrotropin-releasing hormone (TRH) (Lazcano et al., 2015; Müller-Fielitz et al., 2017). However, these studies have not directly investigated whether tanycytes are indeed necessary for regulating these processes. It has thus far not been possible to selectively ablate tanycytes, and to directly observe the resulting effects on metabolism, or any other physiological process. This has been the major obstacle to an accurate understanding of their roles in normal hypothalamic physiology.

The development of transgenic mice that express tamoxifeninducible tanycyte-specific Cre recombinase has made it possible to analyze the acute physiological effects of tanycyte ablation (Pak, Yoo, Miranda-Angulo, Wang, & Blackshaw, 2014). When crossed to mice expressing Cre-dependent *Eno2-lsl-DTA* (Imayoshi et al., 2008), we observed a rapid, selective, and essentially complete ablation of tanycytes of the arcuate nucleus and median eminence (ArcN-ME), which represent all beta-tanycytes, as well as a subset of alpha-2 tanycytes. We have used these mice to directly investigate the role of tanycytes of the ArcN-ME in acute regulation of hypothalamic barrier function, leptin signaling, neurohormone release, fat distribution, insulin sensitivity, and energy balance.

2 | Materials And Methods

2.1 | Animals

Rax-CreERT2 mice generated in the laboratory were crossed with Ai9 (R26-CAG-lsl-tdTom, JAX #007909) (Pak et al., 2014) (JAX#025521), and then bred with *Eno2-lsl-DTA* mice (Kobayakawa et al., 2007) to induce the tanycyte-specific ablation. These mutants were both back-crossed to a C57BL/6 background for at least six generations for all metabolic experiments described here. To induce Cre recombination, the mice were fed with commercial tamoxifen-containing diet (250 mg/kg diet, Envigo Teklad diets #TD.130856) starting at P42 for the indicated periods of time to produce and maintain the tanycyte ablation. This dietary tamoxifen initially lowered body weight, as previously reported (Kiermayer, Conrad, Schneider, Schmidt, & Brielmeier, 2007), and reduced food intake, which was alleviated within 2 weeks although it was ~80% of normal levels (Figure S3). According to a recent study (Ceasrine et al., 2019), oral tamoxifen delivery does not affect either glucose or insulin tolerance in C57BL/6 mice of either sex.

To aid acclimation from regular diet presented at weaning (TD.2018, 3.1 kcal/g; 24 kcal% protein, 18 kcal% fat, 58 kcal% carbohydrate) to the tamoxifen-containing diets, mice were fed from P35 until P42 on a diet that was the same energy density, but with macro-nutrients otherwise matched to the subsequent tamoxifen-containing diet (control diet without tamoxifen: 3.1 kcal/g; 19.7 kcal% protein, 70.6 kcal% carbohydrate, 9.7 kcal% fat; Envigo Teklad diet #TD.07570). For the short-term ablation study, the mice were switched back to this control diet after 3 weeks, for the physiological phenotyping. For the high-fat diet feeding experiments, mice started on a customized tamoxifen diet based on low-fat formulation (Research Diets, 3.8 kcal/g; 20 kcal% protein, 70 kcal% carbohydrate, 10 kcal% fat supplemented with 248 mg/kg diet) for 3 weeks, then were switched to either a very-high-fat diet containing enough tamoxifen to ensure sufficient dosing despite lower intake of grams of this calorie-rich diet (Research Diets, 5.2 kcal/g; 20 kcal% protein, 20 kcal% carbohydrate, 60 kcal% fat, supplemented tamoxifen at 403.1 mg/kg).

Mice were initially housed in a centralized specific pathogen free facility on a 14 hr–10 hr light/dark cycle (07:00 lights on–19:00 lights off). One week prior to physiological studies, mice were transferred to the rodent metabolism core satellite facility at the Center for Metabolism and Obesity Research to acclimate to its vivarium on 12 hr–12 hr light dark cycle (06:00 lights on–18:00 lights off). Climates at both facilities were similar and controlled within temperature (22 ± 1°C) and humidity (45 ± 10%) ranges consistent with the Guide for the Care and Use of Laboratory Animals (eighth ed.). All studies and procedures were performed under a preapproved protocol by the Institutional Animal Care and Use Committee (IACUC) of the Johns Hopkins University School of Medicine.

2.2 | Tissue processing and immunohistochemistry

Mice were anesthetized with intraperitoneal (i.p.) injection of Tribromoethanol/Avertin before transcardial perfusion with 1X PBS followed by 2% paraformaldehyde in 1X PBS. Brains were dissected and postfixed in the same fixative overnight at 4°C. After brief washing with 1X PBS, brains were incubated in 30% sucrose until they sank, then

transferred and incubated in a 50:50 solution of 30% sucrose O.C.T. embedding compound before being frozen. Brains were coronally sectioned at 25 μm thickness using a cryostat (Leica Biosystems) and stored in antifreeze solution at −20°C.

Sections were mounted on Superfrost Plus slides (Fisher Scientific) before immunohistochemistry was conducted, and dried at room temperature for 30 min. For pSTAT3 staining, sections were sequentially incubated with 0.5% NaOH +0.5% H_2O_2 for 20 min, 0.3% glycine for 10 min, and 0.03% SDS for 10 min, and blocked in 4% sheep serum/1% BSA/0.4% Triton X-100 in PBS for 1 hr at room temperature. Otherwise, sections were incubated with sodium citrate buffer (10 mM Sodium citrate, pH 6.0) at 80°C for 30 min for antigen retrieval. After cooling for another 30 min at room temperature, sections were blocked in 10% sheep serum/0.1% Triton X-100 in PBS for 1 hr at room temperature. The sections imaged for Evans Blue staining were immediately treated with blocking solution before primary antibody incubation.

Antibodies used were as follows: rabbit anti-pSTAT3 (1:1000, #9145, Cell Signaling Technology), mouse anti-HuC/D (1:200, #A-21271 Invitrogen), rabbit anti-GFAP (1:500, #Z0334 DAKO), rabbit anti-ZO-1 (1:500, #61–7300 Invitrogen), rat anti-MECA32 (1:200, DSHB), chicken anti-Vimentin (1:1000, #AB5733 Millipore), rat anti-red fluorescent protein (1:500, #5f8–100 Chromo Tek), rabbit anti-DsRed (1:500, #632496 Clontech), mouse anti-Neurofilament-M (1:50, #2H3 DSHB), rabbit anti-Iba1 (1:200, #019–19741 Wako Chemicals), guinea pig anti-NG2 (a kind gift from Dr. Dwight Bergles, The Johns Hopkins University School of Medicine), mouse anti-Acetyl-”-tubulin (1:500, #T6793 Sigma-Aldrich), donkey anti-rabbit Alexa Fluor® 647 (1:500, #711–605-152, Jackson ImmunoResearch), goat anti-mouse IgG, Fc# subclass 2b specific Alexa Fluor® 488 (1:500, #115–545-207, Jackson ImmunoResearch), donkey anti-rabbit Alexa Fluor® 488 (1:500, #711–545-152, Jackson ImmunoResearch), goat anti-chicken Alexa Fluor® 647 (1:500, #A-21449 invitrogen), goat anti-rabbit Alexa Fluor® 555 (1:500, #A-21428 Invitrogen), donkey anti-rat Alexa Fluor® 488 (1:500, #712–545-153 Jackson Immuno-Research), donkey anti-guinea pig Alexa Fluor® 488 (1:500, #706–545-148 Jackson ImmunoResearch).

After counterstaining with DAPI, sections were coverslipped using Vectashield antifade mounting medium (# H-1200, Vector Laboratories) before imaging on a Zeiss LSM 700 Confocal at the Microscope Facility (Johns Hopkins University School of Medicine).

2.3 | In situ hybridization

Chromogenic in situ hybridization was performed on fresh-frozen brain tissue as previously described (Salvatierra et al., 2014; Shimogori et al., 2010). Briefly, coronal 25 μm sections were prepared using a cryostat and fixed with 4% paraformaldehyde. After acetylation with triethanolamine (0.1 M, pH 8.0) and acetic anhydride mixture (0.27%), sections were hybridized with digoxigenin-labeled probes at 70° Covernight. Unbound probes were washed out and sections were blocked with sheep serum followed by incubation with anti-digoxigenin antibodies conjugated to alkaline phosphatase (1:5000) overnight at 4°C. The combination of nitro-blue tetrazolium (NBT) and 5-bromo, 4-chloro, 3-indolylphosphate

(BCIP) was used as chromogenic substrates of alkaline phosphatase. Color development was continued in the same amount of time between wildtype and tanycyte-ablated sections.

2.4 | Evans blue injection

Male mice given 2–3 weeks of reversion to matched control diet, after the 3 weeks of tamoxifen diet, were injected with sterile 1% Evans Blue dye in 0.9% saline through either intravenous (i.v.; 50 μl) or intracerebroventricular (i.c.v.; 2 μl) (Langlet et al., 2013). For i.v. injections, mice were decapitated 20 min after tail vein injections, and brains was dissected and immediately frozen in O.C.T. embedding compound. For i.c.v. injections, Evans Blue is injected into the lateral ventricle (y: −0.3 mm, x: −1 mm, z: 2.5 mm) of anaesthetized mice (100 mg/kg ketamine, 10 mg/kg xylazine, and 3 mg/kg acepromazine) using an infusion pump with 10-μl Hamilton syringe for 1 min. Infusion was confirmed by Evans Blue dye diffusion into the opened cisterna magna during the injection and the needle was removed 1 min after finishing the injection. The snap-frozen brains were coronally sectioned at 25 !m thickness and directly imaged under a fluorescent microscope (Keyence BZ-X700). The sections were then fixed in methanol/acetone (vol/vol) at −20°C for 1 min and further used for immunohistochemistry as described above.

2.5 | Leptin injection

Leptin injection was performed as previously described (Yoo, Cha, Kim, Hoang, & Blackshaw, 2019). Briefly, 3 mg/kg leptin was injected i.p. into male mice and 15 min later transcardial perfusion was performed with 1X PBS followed by 2% paraformaldehyde in 1X PBS. Previous studies of leptin-induced hypothalamic STAT3 phosphorylation studies (Hübschle et al., 2001; Vaisse et al., 1996; Yoo et al., 2019) led us conclude that, if there is any leakage through the opened CSF-hypothalamus or blood-hypothalamus barrier, this would be evident within 15 min following leptin injection.

2.6 | Fasting–refeeding food intake study

Tamoxifen-fed male and female mice were individually housed and initially provided ad libitum access to water and food, in a vivarium on a 12 hr–12 hr light/dark cycle. A wire mesh floor was inserted into the home cage to collect spilled food onto a cage paper beneath the mesh. For the fasting–refeeding experiment, both groups of animals were fasted 18 hr (beginning halfway through the dark phase), and then refed for 24 hr (beginning at the start of the next dark phase). Food intake (corrected for dry, feces-free spillage) was measured at 1-, 3-, 6-, and 24-hr time points during the course of refeeding. The ad libitum food intake data was obtained 1 day prior to the fast–refeed study with the same procedure used for food intake measurement.

2.7 | Luminex assay and ELISA

Mouse serum samples were collected from the tail vein at between 14:00 hr and 16:00 hr. After brief exposure to heat to promote blood vessel dilation, the collection site was cleaned with 70% alcohol, and the mouse is restrained. Blood was collected using a sterile surgical blade (#12–460-440, Fisher Scientific) from the lateral tail vein. Blood flow was stopped by applying pressure with sterile gauze to achieve hemostasis. Metabolic hormone, pituitary

hormone, and neuropeptide serum levels were measured by Luminex assay according to the manufacturer's instructions (#MMHMAG-44K, #MPTMAG-49K, and #RMNPMAG-83K from Millipore Sigma). Serum insulin and testosterone levels were measured using ELISA kit purchased from Millipore (#EZRMI-13K) and Crystal Chem (#80552), respectively. For the acute cold exposure study, mice were transferred to a room maintained at 4°C for 2 hr at between 14:00 hr and 16:00 hr. Blood was briefly collected immediately after cold exposure from the submandibular vein.Serum thyroid-stimulating hormone (TSH) levels were measured using ELISA kit purchased from Cloud-Clone Corp. (#CEA463Mu).

2.8 | Body composition analysis, indirect calorimetry

Fat and lean masses were determined using a whole-body NMR instrument (EchoMRI, Waco, TX) at the Phenotyping Core of the Johns Hopkins University School of Medicine.

Indirect calorimetry was conducted using an Oxymax system (Columbus Instruments), coupled to a temperature- and light-controlled cabinet, in the rodent metabolism core facility at the Center for Metabolism and Obesity Research of the Johns Hopkins University School of Medicine. Male mice were acclimated and monitored in the individual test chambers for 3 days, with a fourth day for data reporting. Daily body weights and food intakes (corrected for spillage) were measured. Oxygen consumption (VO_2, ml/kg/hr) and carbon dioxide production (VCO_2, ml/kg/hr) were measured for each chamber every 10 min. Oxymax software (v. 4.02) calculated RER (VCO_2/VO_2) and energy expenditure ($EE = CV \times VO_2$, $CV = 3.815 + (1.232 \times RER)$.

2.9 | Glucose and insulin tolerance tests

For the glucose tolerance test (GTT), animals were fasted for 12 hr, and 0.1 g/kg glucose was injected i.p. Blood glucose levels during the test were measured using the tail-nick method and a glucometer (Novamax). In addition, up to 25 μl of blood was collected to obtain serum for insulin measurements with an ELISA kit. For the insulin tolerance test (ITT), food was removed 2 hr prior to 0.8 units/kg body weight insulin injection, and blood glucose was measured with a glucometer.

2.10 | Cell counting

All pSTAT3 and HuC/D-double positive cell counts was performed blindly and manually on five sections per brain corresponding to −1.55, −1.67, −1.79, −1.91, −2.15 mm from Bregma. Cell numbers were normalized by the size (mm) of each hypothalamic nucleus measured using ImageJ. The length of tanycytic layer or Evans Blue penetration depth were also measured using ImageJ. All values are expressed as means ± *SEM*.

2.11 | Whole mount staining

Male mice underwent 3 weeks of tamoxifen treatment, followed by a 2–3 week washout period in which they were fed control diet. Mice were sacrificed by cervical dislocation and brains were dissected. Three millimeter-thick coronal slice corresponding to the hypothalamic region containing the third ventricle was obtained using the adult mouse brain matrix (Kent Scientific, CT). This brain slice was carefully dissected to expose the 3V wall in 1xPBS. The whole mount block was fixed by immersion in freshly prepared 4% PFA/

0.1% Triton-X100 in 1!PBS for 10 min and processed for immunostaining as described above.

2.12 | Nissl staining

Brain sections stored in antifreeze solution were mounted on Superfrost Plus slides (Fisher Scientific) and dried at room temperature for 30 min. The slide was pretreated with Xylene (Fisher Scientific, #X5–500), rehydrated through 95 and 70% ethanol to distilled water, and stained in prewarmed 0.1% cresyl violet acetate solution for 15 min. Any excess solution was rinsed quickly with distilled water and sections were dehydrated through 70 and 95% ethanol till 100% ethanol and left in Xylene before being coverslipped with DPX mounting media (Sigma-Aldrich, #06522).

2.13 | Statistical analysis

Throughout all studies, any analyses of more than two groups, affected by two independent factors, were conducted by two-way ANOVA followed by Sidak's test for subsequent pairwise comparisons (Graphpad Prism 7). Analyses of studies with just two groups (genotypes) without additional factors were performed by two-tailed Student's *t* test (Microsoft Excel), unless stated otherwise. A p value <.05 was considered statistically significant.

3 | Results

3.1 | Conditional genetic ablation of hypothalamic tanycytes

To investigate the potential physiological contribution of tanycyte-derived neurogenesis (Kokoeva, Yin, & Flier, 2005; Lee et al., 2012, 2014; Pierce & Xu, 2010), we generated *Rax-CreER;Eno2-lsl-DTA* mice, with the intention of selectively ablating tanycyte-derived neurons without killing the tanycytes themselves, because *Eno2* (gamma-enolase) promoter has been broadly used to derive transgene expression in mature neurons. Analysis of *Eno2* using fISH, however, revealed high levels of *Eno2* mRNA expression in hypothalamic neurons, along with unexpected low levels of expression in both beta- and ventral alpha-2 tanycytes (Figure 1a). Expression of *Eno2* in tanycytes was subsequently confirmed using published scRNA-Seq data (Campbell et al., 2017; Yoo et al., 2019). Because the generation and maturation of neurons in adults is considered a slow process, taking 4–8 weeks (Song, Christian, Ming, & Song, 2012), we focused on here studying the acute physiological effects of tanycyte ablation using *Rax-CreER*; *Eno2-lsl-DTA;Ai9* mice, which would be observed within a short time after ablation.

Loss of tanycytes in *Rax-CreER;Eno2-lsl-DTA;Ai9* mice was observed at ~14–16 days after the start of dietary tamoxifen administration (data not shown). The adult stem cell-like regenerative potential of tanycytes, along with these preliminary data, led us to use a 3-week dietary tamoxifen treatment (Figure 1b,c). This was sufficient to lead to a near-complete ablation of tanycytes in ArcN-ME, as determined by loss of tdTom fluorescence (Student's t test: p = .006, Figure 1d,e). This corresponds to all of the beta-tanycytes and most of the ventral alpha-2 tanycytes, while the alpha-1 and dorsal alpha-2 tanycytes of the ventromedial and dorsomedial hypothalamus were spared as were the ependymal cells of the dorsomedial hypothalamus (Figure 1d,e). Ependymal cells adjacent to the dorsal end of the remaining

alpha-1 tanycytes still maintained pinwheel-like structure and multiple cilia, as shown in whole-mount immunostaining for anti-acetylated-α-tubulin (Figure S1a), suggesting that ependymal cell structure and morphology is maintained following tanycyte ablation.This observation was consistent with the absence of any obvious hydrocephalus (Figure S1b). A glial scar, as measured by increase of GFAP immunostaining, was formed in the ventricular region of the ArcN-ME following tanycyte ablation (Figure 1f).

Loss of tanycyte-specific markers such as *Rax*, *Gpr50*, and *Dio2* was observed in the ArcN-ME (Figure 1g) of tanycyte-ablated (Tny-DTA) mice. However, expression of hypothalamic neuropeptides in hypothalamic regions in direct contact with tanycytes, such as *Npy*, *Cart*, *Gal*, and Sst (Figure S2a), was unaffected. Likewise, the sizes of hypothalamic nuclei which contain tanycytes (ME, ArcN, VMH, and DMH) were unaffected (two-way mixed ANOVA, Figure S2b) and overall axonal projections passing through the ME were not altered (Figure S2c). Furthermore, expression of hypothalamic neurohormones such as Trh, Oxt, and Avp was also unaffected by tanycyte ablation (Figure S2d).

3.2 | ArcN-ME tanycytes are required for maintenance of the CSF-hypothalamus, but not the blood-hypothalamus, barrier

We next investigated whether hypothalamic barrier function was affected by ablation of tanycytes in the ArcN-ME. Previous studies have suggested a role for beta-tanycytes in the formation of the blood-hypothalamus barrier (Mullier et al., 2010; E. M. Rodríguez et al., 2010) and control of its permeability in response to dietary signals (Langlet et al., 2013). Both alpha-2 and beta-tanycytes have also been implicated in formation of the CSF-hypothalamus barrier (Miranda-Angulo, Byerly, Mesa, Wang, & Blackshaw, 2014) and in active transport of small molecules and proteins between the CSF and hypothalamic parenchyma (Frayling et al., 2011; Lazutkaite et al., 2017). We examined the permeability of both the blood-hypothalamus and CSF-hypothalamus barriers in Tny-DTA mice using Evans Blue, delivered via either intravenous (i.v.) or intracerebroventricular (i.c.v) injection (Mullier et al., 2010). Tny-DTA mice showed no difference in blood-hypothalamic barrier permeability, as measured by Evan Blue staining after i.v. delivery, with reduced absolute levels of ME staining which mainly reflected the overall reduction in ME volume that is seen in Tny-DTA mice (Figure 2a,b). In contrast, i.c.v. delivery of Evans Blue demonstrated substantially increased permeability in ArcN of Tny-DTA mice, while the staining in the ME was still strong near the ventricular floor (Figure 2c,d).

Immunostaining for the tight junction marker ZO-1, which is expressed in tanycytes and reported to maintain hypothalamic barrier function, is lost in both ArcN and ME tanycytes in *Rax-CreER*; *Eno2-lsl-DTA* mice (Figure 2e,f). In contrast, vimentin immunoreactivity is increased in the ventricular zone of the ME (Figure 2e′,f′), which overlaps with the GFAP immunostaining but shows a more restricted distribution (Figure 1f). Immunostaining for MECA32, a marker of fenestrated capillaries, revealed no change in the number of immuno-positive cells in ME between the two groups (Figure 2g,h). Together, these data demonstrate that, while tanycytes are necessary for maintenance of the CSF-hypothalamus barrier, they are not required to maintain the blood-hypothalamus barrier.

A previous report suggested that beta-2 tanycytes were involved in active transcytosis of leptin from blood to the hypothalamus (Balland et al., 2014). However, our recent study demonstrated that leptin receptors are not detectable in tanycytes, and are not required for leptin transport into hypothalamus (Yoo et al., 2019). To further investigate whether tanycytes of the ArcN-ME might regulate hypothalamic leptin signaling, we performed intraperitoneal (i.p.) leptin injection in both control and Tny-DTA mice. We observed no differences in pSTAT3 staining in neurons of any hypothalamic regions containing or in direct contact with tanycytes (Figure 3a,b). These data further indicate that tanycytes are not involved in active transport of leptin from blood to the hypothalamus, or at least indicate that such a route is dispensable for leptin transport into the hypothalamus.

3.3 | Ablation of ArcN-ME tanycytes led to adiposity without body weight change in male mice

To more broadly investigate the contribution of tanycytes of the ArcN-ME to energy balance and other metabolic outcomes, we first analyzed food intake and body weight in control and Tny-DTA mice. Tamoxifen administration, via inclusion in a low-fat diet fed ad libitum, led initially to weight loss associated with reduced food intake, as previously reported (Kiermayer et al., 2007; Figure 4b,c). The initial reduction in food intake largely resolved after 2 weeks of tamoxifen exposure in both male and female mice, regardless of genotype (Figure S3). To investigate the potential cumulative effects of loss of both tanycytes and tanycyte-derived cells, in both male and female mice, we initially used a prolonged tamoxifen treatment. Both control and Tny-DTA mice were fed dietary tamoxifen for a period of over 50 days (Figure 4a, top bar). Although there was only a trend toward increase in body weight in Tny-DTA mice compared to wildtypes (Figure 4b, green), Tny-DTA mice did have significantly more fat mass than wildtype mice after 7 weeks on the diet ($p < .001$, Figure 4d, green bars), an outcome that was not observed at the earlier 4-week time point ($p = .129$, Figure 4d, green patterned bars). Specifically, male Tny-DTA mice had substantially more perigonadal fat (Student's t test: $p = .013$, Figure 4f,g). No significant increase in fat mass was observed in female mice (Student's t test: $p = .172$, Figure S4a–c).

These results from longer-term tanycyte ablation prompted us to investigate whether the effect was the result of acute tanycyte ablation, or if it required cumulative effects of long-term ablation. We fed tanycyte-ablated and wildtype mice low-fat diet containing tamoxifen for 3 weeks (Figure 4a, middle bar, also as described in Figure 1b). There were no differences in body weight between male Tny-DTA mice and wildtypes, either during 3 weeks of low-fat diet containing tamoxifen, or during two subsequent weeks back on control diet without tamoxifen (Figure 4c). When mice were exposed to tamoxifen for only 3 weeks, the Tny-DTA mice already showed significantly increased fat mass at the fourth week compared with wildtype mice ($p = .02$, Figure 4d, blue bars), whereas in the longer-term study this effect was still not significant, despite the additional week of tamoxifen exposure ($p = .103$, Figure 4d, green patterned bars). An increased opportunity for fat gain may have occurred in the short-term study due to the removal of tamoxifen, and of its continued ability to moderately suppress food intake, as evident by the rapid increase in body weight in both groups of mice (Figure 4c).

Tny-DTA mice had significantly more fat than wildtype mice (Figure 4d). We found no significant difference in lean body mass in any groups fed with regular tamoxifen diet (two-way ANOVA, Figure 4e), and body weights of Tny-DTA were not significantly greater than those of wildtype mice, implying that the increase in fat mass, though statistically significant, is modest. These results were confirmed by terminal measures of dissected fat pads (Figure 4g). Tny-DTA mice had increased perigonadal and retroperitoneal fat pads (Student's t test: $p = .024$ and $p = .029$, respectively), with a similar trend also seen for inguinal fat ($p = .05$). Perigonadal adipocytes were larger in Tny-DTA mice than in wildtype mice (Figure 4h). We did not find significant differences in brown adipose tissue mass (Student's *t* test: $p = .578$, Figure 4g) or in the sizes of any other internal organs, between the two mouse groups (data not shown).

3.4 | ArcN-ME tanycyte-ablated male mice had increased fasting-induced food intake and decreased insulin sensitivity

To explore responses to states of negative and positive energy balance, we measured food intake in control and Tny-DTA mice fed ad libitum, and then refed after an overnight food deprivation, during the long-term ablation study (Figure 4a, top bar). In male mice maintained on tamoxifen for 4 weeks, no differences in food intake were observed in mice fed ad libitum, or during refeeding after the fast (Figure 4i), indicating that food intake was not affected in the early phase of fat accumulation. However, after 8 weeks of tamoxifen treatment, male Tny-DTA mice showed hyperphagia, particularly in response to food deprivation (Figure 4j).

To further investigate mechanisms that might contribute to the hyperphagia, we analyzed blood hormone levels in male mice subjected to both long- and short-term tamoxifen treatments (Figures S5 and S6, respectively). Tny-DTA mice that underwent either long-term or short-term tamoxifen treatment showed significant increase in serum leptin (Student's t test: $p = .037$ and $p = .007$, respectively, Figures S5a and S6a), consistent with the increased fat content. Pancreatic polypeptide (PP) and peptide YY (PYY), satiety hormones from the digestive system, were increased significantly in Tny-DTA mice following long-term tamoxifen treatment (Student's *t* test: $p = .018$ and $p = .044$, respectively, Figure S5c,d), but no change in serum insulin was observed (Student's *t* test: $p = .539$ and $p = .859$, respectively, Figures S5b and S6b). No changes were observed in serum levels of leptin and insulin in females (Student's *t* test: $p = .816$ and $p = .733$, respectively, Figure S7a,b).

Glucose tolerance was not affected after tanycyte ablation induced by short-term or long-term tamoxifen treatments (Figure 4k, m). However, tanycyte-ablated male mice exhibited substantially decreased sensitivity to insulin after long-term tamoxifen treatment (Figure 4l), consistent with the increased adiposity in these animals. While short-term tamoxifen treatment initially did not appear to affect insulin sensitivity (data not shown), we have noticed that the baseline glucose levels in these animals tend to low (Figure 4n, left panel), and observed that insulin sensitivity was significantly decreased when initial glucose levels are normalized (Figure 4n, right panel). In contrast, females exhibited no differences in food intake, glucose tolerance, or insulin sensitivity (Figure S4d–g).

To further investigate the mechanisms mediating the acute increase in fat content, and to test the more general role of tanycytes in regulation of release of hypothalamic and pituitary hormones, we expanded our analysis to test serum levels of a broad panel of factors (Figures S5, S6, and S7). Surprisingly, few consistent changes in hormone levels were observed. Small but statistically significant increases in serum TSH and neurotensin levels were observed in Tny-DTA mice following short-term treatment (Student's *t* test: $p = .048$ and $p = .046$, respectively, Figure S6l,q), although neither of the hormones was affected in Tny-DTA mice following long-term tamoxifen treatment (Figure S5l,q).

Because tanycytes produce thyroid hormone converting enzyme (Yasuo, Yoshimura, Ebihara, & Korf, 2007), and have been linked to regulation of TRH release from hypothalamic neurosecretory cells (Lazcano et al., 2015; Müller-Fielitz et al., 2017; Sánchez et al., 2009), we further investigated whether short-term tanycyte-ablation compromised the response of the hypothalamic–pituitary–thyroid (HPT) axis to an acute cold challenge (Figure S8). Serum TSH level was measured before and after 2-hr 4°C exposure from 17 wildtype and 21 Tny-DTA mice. Temperature change significantly exerted a main effect on TSH concentration ($p < .001$), but which did not depend on genotype ($p = .488$). However, further pairwise comparison revealed that serum TSH levels were significantly elevated following 2-hr cold exposure in the Tny-DTA mice ($p = .009$), while the control group only showed the tendency to an increase ($p = .071$). Decreased serum oxytocin levels were observed in Tny-DTA mice following long-term tamoxifen treatment (Student's t test: $p = .008$, Figure S5o). No changes were observed in serum hormone levels in females (Figure S7), with the surprising exception of growth hormone (GH), which showed twofold higher levels following tanycyte-ablation (Student's *t* test: $p < .001$, Figure S7m). Since females do not show an overall increase in body weight or lean mass, the significance of this observation is unclear.

3.5 | Effects of high-fat diet on tanycyte-deficient male mice

The increased fat content and decreased insulin sensitivity in tanycyte-deficient mice that had been fed a low-fat diet raised the possibility that these effects might be enhanced on an obesogenic high-fat diet (HFD). To address this, we placed both control and tanycyte-ablated male mice on a high-fat diet immediately following 3 weeks of feeding with tamoxifen-supplemented low-fat diet (Figure 4a, bottom bar). Tny-DTA mice showed a trend toward increase in body weight gain on HFD compared with control mice (Figure 4b, orange). Both HFD and genotype had a significant main effect on fat mass ($p < .0001$ and $p = .034$, respectively in Figure 4d, orange), with a trend toward an interaction between these two factors ($p = .059$). Further pairwise comparison confirmed that HFD produced a robust increase in overall fat mass in both groups (WT: $p < .0001$, Tny-DTA: $p < .0001$) and that, after HFD, Tny-DTA mice showed statistically greater fat mass than wildtype mice ($p = .011$), which had not been evident before introduction of HFD ($p = .526$). However, the increased fat mass overall in Tny-DTA mice was not apparent with terminal measures of individual depots of white adipose tissue (gonadal: $p = .925$, inguinal: $p = .353$, retroperitoneal: $p = .607$, Figure 4g, orange), in contrast to the substantial increases seen in Tny-DTA mice maintained on regular low-fat tamoxifen diet (Figure 4g, green and blue). Genotype, but not HFD feeding, had a significant main effect on lean mass ($p = .01$, Figure

4e). Further pairwise tests did not reveal any significant differences in lean mass between genotypes either before ($p = .127$) or after HFD ($p = .125$).

Unlike ablated mice maintained only on low-fat tamoxifen diet (Figure 4k,m), HFD-fed tanycyte-deficient mice showed slight but significant improvement in glucose tolerance at early time points during a GTT (Figure 4o), as well as transiently increased serum insulin levels 15 min after glucose injection (data not shown). Tanycyte-ablated male mice on HFD showed prolonged effects of insulin action in an ITT (Figure 4p) suggesting a decreased counterregulatory response to hypoglycemia relative to wildtype mice. Thus, the overall effect of HFD in Tny-DTA mice was more moderate than that observed on the regular tamoxifen diet, where differences in insulin sensitivity were observed at earlier time points (Figure 4l).

3.6 | Thermoneutrality enhances fat accumulation in tanycyte-ablated mice

To further investigate the mechanism underlying the adiposity observed in Tny-DTA mice, we conducted indirect calorimetry studies on male mice that had undergone short-term tanycyte ablation (Figure 5a). At a 4-week time point when Tny-DTA mice start to show increased fat mass (Student t test: $p < .03$,Figure 4d, blue bars), but no differences in body weight or caloric intake (Figure 4c,i), we noticed a subtle shift away from the fat oxidation that ordinarily takes place starting in the latter part of the dark phase and continues throughout the light phase (Figure 5i, upper panel). Two weeks of cold exposure during the development of adiposity in Tny-DTA mice did not alter the upward trend in fat mass in Tny-DTA mice (Figure 5c), although this did lose statistical significance (Student's t test: $p = .139$), consistent with a lack of difference from control mice in respiratory exchange ratio (RER) during the photoperiod (Figure 5i, middle panel). In contrast, testing under thermoneutral condition dramatically enhanced the difference in RER between controls and Tny-DTA mice, particularly during the light phase, with Tny-DTA mice exhibiting a shift away from the fat burning that ordinarily occurs during the light phase (Figure 5i, bottom panel). Although Tny-DTA mice showed differences from wild type mice in RER during thermoneutrality and to some degree at normal room temperature, these effects did not result in any change in energy expenditure. Energy expenditure was affected by temperature as expected, for both genotypes, with an overall increase under cold conditions and overall decrease with thermoneutrality (Figure 5j).

Both temperature and genotype had significant main effects on fat mass ($p < .0001$ and $p = .001$, respectively in Figure 5c) without significant interaction between these two factors ($p = .632$). Subsequent multiple comparison revealed a statistically significant increase in fat mass of Tny-DTA mice compared with wild type mice only at thermoneutrality ($p = .036$), resulting in a significant increase in body weight (Student's t test: $p = .039$, Figure 5b, orange). Temperature had a significant main effect on both food intake and lean mass ($p < .0001$ in both cases, Figure 5d,e), but these were not affected by genotype (food intake: $p = .09$, lean mass: $p = .8766$). However, we found a trend toward increased food intake in the Tny-DTA mice under thermoneutrality ($p = .08$, Figure 5e, orange), suggesting that it might make a minor contribution to the increased fat mass.

At thermoneutrality, Tny-DTA mice showed larger adipocytes in inguinal white adipose tissue (iWAT) compared to controls (Figure 5f, middle panel), although this effect did not reach statistical significance (Figure 5g). Wildtype mice under thermoneutrality did have fat droplets in intrascapular brown adipose tissue (BAT), consistent with low or no fat burning for heat generation by BAT under this condition. In comparison, Tny-DTA mice had even larger fat droplets in BAT than wild type animals (Figure 5f, right panel; Figure 5h).

4 | Discussion

In this study, we have investigated the cellular and physiological effects of selective ablation of tanycytes of the ArcN and ME. Although tanycytes in these hypothalamic regions have been proposed to control a broad range of physiological processes, including blood-hypothalamic barrier formation, control of hypothalamic leptin signaling and regulation of the neuroendocrine axis, our findings revealed surprisingly subtle phenotypes in tanycyte-ablated mice, which are primarily restricted to a male-specific increase in adiposity and a decreased insulin sensitivity, without significant body weight change.

Perhaps most surprisingly, complete ablation of beta-tanycytes did not lead to an increased permeability of the blood-hypothalamus barrier, whereas it led to a clear increase of Evans Blue permeability from the CSF into the ArcN parenchyma, along with minor leakage into the ME. This is consistent with a previous report that tanycytes regulate CSF-hypothalamic barrier function (Miranda-Angulo et al., 2014). This likely implies a central role for other cell types, such as endothelial cells and pericytes, in regulating permeability between the ArcN and ME. The finding that hypothalamic leptin signaling was unaffected by absence of beta-tanycytes is consistent with our recent findings that LepR expression in tanycytes is not necessary for leptin transport from blood to hypothalamic parenchyma (Yoo et al., 2019). NG2-positive oligodendrocyte progenitors, which are reported to have a critical role in regulating leptin signaling in the ME (Djogo et al., 2016), were likewise not significantly changed in number or distribution in tanycyte-ablated mice compared with controls (Figure S9b). Ependymal cells are another cell type known to express leptin receptors and which shows strong and immediate changes in gene expression in response to leptin injection (Yoo et al., 2019). Tanycyte-ablated mice seem to have morphologically and functionally intact ependymal cells; it remains formally possible that ependymal cells may compensate for any defects in leptin transport resulting directly or indirectly from tanycyte ablation.

We likewise observed only modest and transient effects on the neuroendocrine axis. Beta-tanycytes have been implicated in active regulation of both gonadotropin-releasing hormone (GnRH) and TRH synthesis and/or release (Müller-Fielitz et al., 2017; Parkash et al., 2015; Sánchez et al., 2009). Tanycyte foot processes have been reported to physically inhibit GnRH release in females, but retract during estrus to allow GnRH release into the portal circulation (de Seranno et al., 2010; Parkash et al., 2015). While we did not observe significant changes in serum levels of FSH or LH in either sex, these results are difficult to interpret due to disruptive effects of prolonged tamoxifen exposure on the hypothalamic–pituitary–gonadal axis.

Beta-tanycytes strongly express *Dio2*, an enzyme that converts T4 to T3, which is known to negatively regulate transcription of *Trh* (de Vries et al., 2016). Furthermore, beta-tanycytes release exoenzymes which degrade TRH (Lazcano et al., 2015; Sánchez et al., 2009). One might therefore predict that ablation of beta-tanycytes would lead to a global activation of the HPT axis (Marsili et al., 2011). We did not, however, observe any obvious changes in hypothalamic Trh expression in tanycyte-ablated mice (Figure S2). While we observed an increase in serum TSH in male mice subjected to short-term tanycyte ablation (Figure S6l), consistent with HPT hyperactivation, no significant change in serum TSH was observed in either male mice subjected to longer-term tanycyte ablation or in female mice (Figures S5l and S7k). Serum levels of TSH were significantly induced by acute cold exposure in tanycyte-ablated mice (Figure S8) (Sánchez et al., 2009), supporting the possible role of beta-tanycytes in negative regulation of the HPT axis. However, the overall results suggest that any role of tanycytes play in regarding the HPT axis is relatively modest, sex-specific, and that the functional disruption is rapidly compensated for by changes in other tissues.

Beta-tanycytes have been reported to sense glucose and amino acids (Benford et al., 2017; Frayling et al., 2011; Lazutkaite et al., 2017), and have been proposed to act as essential central integrators of metabolic regulation (Ebling & Lewis, 2018; García-Cáceres et al., 2019; Prevot et al., 2018). Tanycyte-ablated mice did not show changes in overall body weight or food intake in the 4 weeks following tanycyte ablation. However, we observed a statistically significant increase in adiposity, that is most prominent in visceral fat, in male mice at this stage (Figure 4d,f,g). We also noticed a trend toward reduction in lean mass, explaining why no overall change in body weight was observed (Figure 4e). Within 6 weeks following tanycyte ablation in male mice, decreased insulin sensitivity was observed, along with increased serum leptin levels (Figures 4n and S5a), consistent with the increased adiposity. However, glucose tolerance was unaffected (Figure 4m), suggesting that the pancreas may secrete more insulin to achieve normal glucose homeostasis. In females, no significant changes in adiposity, serum leptin and insulin sensitivity were observed (Figures S4 and S7a).

The molecular mechanisms underlying these acute metabolic changes and their sexual dimorphism are as yet unclear. It is noteworthy that females have better insulin sensitivity than males, mainly due to higher insulin sensitivity in their adipose tissue, particularly in visceral fat depot where we see the largest differences in adiposity in the male tanycyte-deficient mice (Macotela, Boucher, Tran, & Kahn, 2009). It appears unlikely that tanycyte ablation results in increased hypothalamic inflammation, widely proposed to play a role in driving high-fat diet-induced obesity, because the number and distribution of microglia in the hypothalamus of tanycyte-ablated mice are not different than those of control mice, and the ramified morphology indicates that hypothalamic microglia are in resting state (Figure S9a) (Li & Barres, 2018; Rahman, Kim, Lee, Yu, & Suk, 2019; Thaler et al., 2012). However, the data suggest that there is a direct or indirect involvement of tanycytes in control of fat utilization, as shown by the slightly higher RER overall during typically fat-oxidizing phases of the photoperiod in tanycyte-deficient male mice (Figure 5i), which is clearly unmasked when mice are housed at thermoneutrality.

Increased adiposity in males became more prominent at 7 weeks following tanycyte ablation although overall body weight was not significantly affected (Figure 4b,d). This was accompanied by an exacerbated hyperphagic response to prolonged fasting, although ad libitum food intake was largely unaffected (Figure 4j). This enhanced refeeding implies that longer-term tanycyte ablation disrupts both normal central integration and the response to signals of negative energy balance. This could result from a variety of mechanisms, ranging from the absence of sensation of small molecules by tanycytes to the disruption of generation of tanycyte-derived neurons or glia (Lazutkaite et al., 2017; Martínez, Cifuentes, Tapia, & Nualart, 2019; Yoo & Blackshaw, 2018).

In conclusion, tanycytes of the ArcN-ME have can influence fat metabolism, but are not essential for regulation of food intake and overall body weight control, as has been implied by recent studies (R. J. Elizondo-Vega et al., 2019; Müller-Fielitz et al., 2017; Prevot et al., 2018). This does not rule out a potentially important role for tanycytes in influencing these processes, but demonstrates that other cells can compensate for the loss of tanycyte function. It also remains possible that the residual tanycytes, which would be alpha-1 and a dorsally located subset of alpha-2 subtypes, could be major players in the expected metabolic phenotypes (Barahona et al., 2018; R. Elizondo-Vega et al., 2016). Furthermore, we have only tested a limited number of potential environmental conditions, and a more prominent role for tanycytes may be revealed in response to other physiological challenges. Finally, there are many other physiological processes that may be tanycyte-regulated that were not tested in this study. Notably, tanycytes have been reported to play a critical role in biological timing and reproductive regulation in species that show strong photoperiodism (Dardente & Lomet, 2018; Helfer, Barrett, & Morgan, 2019; Sáenz de Miera, 2019), and it is possible that related behaviors may be under tanycyte-dependent regulation in mice.

Supplementary Material

Refer to Web version on PubMed Central for supplementary material.

Acknowledgments

We thank Dr Shigeyoshi Itohara for generously providing the *Eno2-lsl-DTA* mice. We thank Dr D. Bergles for the kind gift of the anti-NG2 antibody. We thank W. Yap, J. Ling, T. Hoang, and C. Santiago for their comments on the manuscript. This work was supported by grant DK108230 to S.B. and a Maryland Stem Cell Postdoctoral Research Fellowship to S.Y.

Funding information

Maryland Stem Cell Research Fund, Grant/ Award Number: Post Doctoral Fellowship; National Institute of Diabetes and Digestive and Kidney Diseases, Grant/Award Number: DK108230

References

Balland E, Dam J, Langlet F, Caron E, Steculorum S, Messina A, … Prévot V (2014). Hypothalamic tanycytes are an ERK-gated conduit for leptin into the brain. Cell Metabolism, 19(2), 293–301. 10.1016/j.cmet.2013.12.015 [PubMed: 24506870]

Barahona MJ, Llanos P, Recabal A, Escobar-Acuña K, Elizondo-Vega R, Salgado M, … García-Robles MA (2018). Glial hypothalamic inhibition of GLUT2 expression alters satiety, impacting eating behavior. Glia, 66(3), 592–605. 10.1002/glia.23267 [PubMed: 29178321]

Benford H, Bolborea M, Pollatzek E, Lossow K, Hermans-Borgmeyer I, Liu B, … Dale N (2017). A sweet taste receptor-dependent mechanism of glucosensing in hypothalamic tanycytes. Glia, 65(5), 773–789. 10.1002/glia.23125 [PubMed: 28205335]

Campbell JN, Macosko EZ, Fenselau H, Pers TH, Lyubetskaya A, Tenen D, … Tsai LT (2017). A molecular census of arcuate hypothalamus and median eminence cell types. Nature Neuroscience, 20(3), 484–496. 10.1038/nn.4495 [PubMed: 28166221]

Ceasrine AM, Ruiz-Otero N, Lin EE, Lumelsky DN, Boehm ED, & Kuruvilla R (2019). Tamoxifen improves glucose tolerance in a delivery-, sex-, and strain-dependent manner in mice. Endocrinology, 160(4), 782–790. 10.1210/en.2018-00985 [PubMed: 30759201]

Dardente H, & Lomet D (2018). Photoperiod and thyroid hormone regulate expression of l-dopachrome tautomerase (Dct), a melanocyte stem-cell marker, in tanycytes of the ovine hypothalamus. Journal of Neuroendocrinology, 30(9), e12640 10.1111/jne.12640 [PubMed: 30129070]

de Seranno S, d'Anglemont de Tassigny X, Estrella C, Loyens A, Kasparov S, Leroy D, … Prevot V (2010). Role of estradiol in the dynamic control of tanycyte plasticity mediated by vascular endothelial cells in the median eminence. Endocrinology, 151(4), 1760–1772. 10.1210/en.2009-0870 [PubMed: 20133455]

de Vries EM, Nagel S, Haenold R, Sundaram SM, Pfrieger FW, Fliers E, … Boelen A (2016). The role of hypothalamic NF-%B signaling in the response of the HPT-Axis to acute inflammation in female mice. Endocrinology, 157(7), 2947–2956. 10.1210/en.2016-1027 [PubMed: 27187176]

Djogo T, Robins SC, Schneider S, Kryzskaya D, Liu X, Mingay A, … Kokoeva MV (2016). Adult NG2-glia are required for median Eminence-mediated leptin sensing and body weight control. Cell Metabolism, 23(5), 797–810. 10.1016/j.cmet.2016.04.013 [PubMed: 27166944]

Ebling FJP, & Lewis JE (2018). Tanycytes and hypothalamic control of energy metabolism. Glia, 66(6), 1176–1184. 10.1002/glia.23303 [PubMed: 29411421]

Elizondo-Vega R, Cortés-Campos C, Barahona MJ, Carril C, Ordenes P, Salgado M, … García-Robles M. d. L. A. (2016). Inhibition of hypothalamic MCT1 expression increases food intake and alters orexigenic and anorexigenic neuropeptide expression. Scientific Reports, 6, 33606 10.1038/srep33606 [PubMed: 27677351]

Elizondo-Vega R, Cortes-Campos C, Barahona MJ, Oyarce KA, Carril CA, & García-Robles MA (2015). The role of tanycytes in hypothalamic glucosensing. Journal of Cellular and Molecular Medicine, 19(7), 1471–1482. 10.1111/jcmm.12590 [PubMed: 26081217]

Elizondo-Vega RJ, Recabal A, & Oyarce K (2019). Nutrient sensing by hypothalamic Tanycytes. Frontiers in Endocrinology, 10, 244 10.3389/fendo.2019.00244 [PubMed: 31040827]

Frayling C, Britton R, & Dale N (2011). ATP-mediated glucosensing by hypothalamic tanycytes. The Journal of Physiology, 589(Pt 9), 2275–2286. 10.1113/jphysiol.2010.202051 [PubMed: 21486800]

García-Cáceres C, Balland E, Prevot V, Luquet S, Woods SC, Koch M, … Tschöp MH (2019). Role of astrocytes, microglia, and tanycytes in brain control of systemic metabolism. Nature Neuroscience, 22(1), 7–14. 10.1038/s41593-018-0286-y [PubMed: 30531847]

Haan N, Goodman T, Najdi-Samiei A, Stratford CM, Rice R, El Agha E, … Hajihosseini MK (2013). Fgf10-expressing tanycytes add new neurons to the appetite/energy-balance regulating centers of the postnatal and adult hypothalamus. *The Journal of Neuroscience*: The Official Journal of the Society for Neuroscience, 33(14), 6170–6180. 10.1523/JNEUROSCI.2437-12.2013

Helfer G, Barrett P, & Morgan PJ (2019). A unifying hypothesis for control of body weight and reproduction in seasonally breeding mammals. Journal of Neuroendocrinology, 31(3), e12680 10.1111/jne.12680 [PubMed: 30585661]

Hübschle T, Thom E, Watson A, Roth J, Klaus S, & Meyerhof W (2001). Leptin-induced nuclear translocation of STAT3 immunoreactivity in hypothalamic nuclei involved in body weight regulation. The Journal of Neuroscience: The Official Journal of the Society for Neuroscience, 21(7), 2413–2424. [PubMed: 11264315]

Imayoshi I, Sakamoto M, Ohtsuka T, Takao K, Miyakawa T, Yamaguchi M, … Kageyama R (2008). Roles of continuous neurogenesis in the structural and functional integrity of the adult forebrain. Nature Neuroscience, 11(10), 1153–1161. 10.1038/nn.2185 [PubMed: 18758458]

Kiermayer C, Conrad M, Schneider M, Schmidt J, & Brielmeier M (2007). Optimization of spatiotemporal gene inactivation in mouse heart by oral application of tamoxifen citrate. Genesis, 45(1), 11–16. 10.1002/dvg.20244 [PubMed: 17216603]

Kobayakawa K, Kobayakawa R, Matsumoto H, Oka Y, Imai T, Ikawa M, … Sakano H (2007). Innate versus learned odour processing in the mouse olfactory bulb. Nature, 450(7169), 503–508. 10.1038/nature06281 [PubMed: 17989651]

Kokoeva MV, Yin H, & Flier JS (2005). Neurogenesis in the hypothalamus of adult mice: Potential role in energy balance. Science, 310 (5748), 679–683. 10.1126/science.1115360 [PubMed: 16254185]

Langlet F, Levin BE, Luquet S, Mazzone M, Messina A, Dunn-Meynell AA, … Dehouck B (2013). Tanycytic VEGF-A boosts blood-hypothalamus barrier plasticity and access of metabolic signals to the arcuate nucleus in response to fasting. Cell Metabolism, 17(4), 607–617. 10.1016/j.cmet.2013.03.004 [PubMed: 23562080]

Lazcano I, Cabral A, Uribe RM, Jaimes-Hoy L, Perello M, Joseph-Bravo P, … Charli J-L (2015). Fasting enhances Pyroglutamyl peptidase II activity in Tanycytes of the Mediobasal hypothalamus of male adult rats. Endocrinology, 156(7), 2713–2723. 10.1210/en.2014-1885 [PubMed: 25942072]

Lazutkaite G, Soldà A, Lossow K, Meyerhof W, & Dale N (2017). Amino acid sensing in hypothalamic tanycytes via umami taste receptors. Molecular Metabolism, 6(11), 1480–1492. 10.1016/j.molmet.2017.08.015 [PubMed: 29107294]

Lee DA, Bedont JL, Pak T, Wang H, Song J, Miranda-Angulo A, … Blackshaw S (2012). Tanycytes of the hypothalamic median eminence form a diet-responsive neurogenic niche. Nature Neuroscience, 15(5), 700–702. 10.1038/nn.3079 [PubMed: 22446882]

Lee DA, Yoo S, Pak T, Salvatierra J, Velarde E, Aja S, & Blackshaw S (2014). Dietary and sex-specific factors regulate hypothalamic neurogenesis in young adult mice. Frontiers in Neuroscience, 8, 157 10.3389/fnins.2014.00157 [PubMed: 24982613]

Li Q, & Barres BA (2018). Microglia and macrophages in brain homeostasis and disease. Nature Reviews. Immunology, 18(4), 225–242. 10.1038/nri.2017.125

Macotela Y, Boucher J, Tran TT, & Kahn CR (2009). Sex and depot differences in adipocyte insulin sensitivity and glucose metabolism. Diabetes, 58(4), 803–812. 10.2337/db08-1054 [PubMed: 19136652]

Marsili A, Sanchez E, Singru P, Harney JW, Zavacki AM, Lechan RM, & Larsen PR (2011). Thyroxine-induced expression of pyroglutamyl peptidase II and inhibition of TSH release precedes suppression of TRH mRNA and requires type 2 deiodinase. The Journal of Endocrinology, 211(1), 73–78. 10.1530/JOE-11-0248 [PubMed: 21788297]

Martínez F, Cifuentes M, Tapia JC, & Nualart F (2019). The median eminence as the hypothalamic area involved in rapid transfer of glucose to the brain: Functional and cellular mechanisms. Journal of Molecular Medicine, 97, 1085–1097. 10.1007/s00109-019-01799-5 [PubMed: 31129757]

Miranda-Angulo AL, Byerly MS, Mesa J, Wang H, & Blackshaw S (2014). Rax regulates hypothalamic tanycyte differentiation and barrier function in mice. The Journal of Comparative Neurology, 522(4), 876–899. 10.1002/cne.23451 [PubMed: 23939786]

Müller-Fielitz H, Stahr M, Bernau M, Richter M, Abele S, Krajka V, … Schwaninger M (2017). Tanycytes control the hormonal output of the hypothalamic-pituitary-thyroid axis. Nature Communications, 8(1), 484 10.1038/s41467-017-00604-6

Mullier A, Bouret SG, Prevot V, & Dehouck B (2010). Differential distribution of tight junction proteins suggests a role for tanycytes in blood-hypothalamus barrier regulation in the adult mouse brain. The Journal of Comparative Neurology, 518(7), 943–962. 10.1002/cne.22273 [PubMed: 20127760]

Pak T, Yoo S, Miranda-Angulo AL, Wang H, & Blackshaw S (2014). Rax-CreERT2 knock-in mice: A tool for selective and conditional gene deletion in progenitor cells and radial glia of the retina and hypothalamus. PLoS One, 9(4), e90381 10.1371/journal.pone.0090381 [PubMed: 24699247]

Parkash J, Messina A, Langlet F, Cimino I, Loyens A, Mazur D, … Giacobini P (2015). Semaphorin7A regulates neuroglial plasticity in the adult hypothalamic median eminence. Nature Communications, 6, 6385 10.1038/ncomms7385

Pierce AA, & Xu AW (2010). De novo neurogenesis in adult hypothalamus as a compensatory mechanism to regulate energy balance. The Journal of Neuroscience: The Official Journal of the Society for Neuroscience, 30(2), 723–730. 10.1523/JNEUROSCI.2479-09.2010

Prevot V, Dehouck B, Sharif A, Ciofi P, Giacobini P, & Clasadonte J (2018). The versatile Tanycyte: A hypothalamic integrator of reproduction and energy metabolism. Endocrine Reviews, 39(3), 333–368. 10.1210/er.2017-00235 [PubMed: 29351662]

Rahman MH, Kim M-S, Lee I-K, Yu R, & Suk K (2019). Corrigendum: Interglial crosstalk in obesity-induced hypothalamic inflammation. Frontiers in Neuroscience, 13, 3 10.3389/fnins.2019.00003 [PubMed: 30728761]

Rodríguez E, Guerra M, Peruzzo B, & Blázquez JL (2019). Tanycytes: A rich morphological history to underpin future molecular and physiological investigations. Journal of Neuroendocrinology, 31(3), e12690 10.1111/jne.12690 [PubMed: 30697830]

Rodríguez EM, Blázquez JL, & Guerra M (2010). The design of barriers in the hypothalamus allows the median eminence and the arcuate nucleus to enjoy private milieus: The former opens to the portal blood and the latter to the cerebrospinal *fluid*. Peptides, 31(4), 757–776. 10.1016/j.peptides.2010.01.003 [PubMed: 20093161]

Sáenz de Miera C (2019). Maternal photoperiodic programming enlightens the internal regulation of thyroid-hormone deiodinases in tanycytes. Journal of Neuroendocrinology, 31(1), e12679 10.1111/jne.12679 [PubMed: 30585670]

Salvatierra J, Lee DA, Zibetti C, Duran-Moreno M, Yoo S, Newman EA, … Blackshaw S (2014). The LIM homeodomain factor Lhx2 is required for hypothalamic tanycyte specification and differentiation. *The Journal of Neuroscience*: The Official Journal of the Society for Neuroscience, 34(50), 16809–16820. 10.1523/JNEUROSCI.1711-14.2014

Sánchez E, Vargas MA, Singru PS, Pascual I, Romero F, Fekete C, … Lechan RM (2009). Tanycyte pyroglutamyl peptidase II contributes to regulation of the hypothalamic-pituitary-thyroid axis through glial-axonal associations in the median eminence. Endocrinology, 150 (5), 2283–2291. 10.1210/en.2008-1643 [PubMed: 19179432]

Shimogori T, Lee DA, Miranda-Angulo A, Yang Y, Wang H, Jiang L, … Blackshaw S (2010). A genomic atlas of mouse hypothalamic development. Nature Neuroscience, 13(6), 767–775. 10.1038/nn.2545 [PubMed: 20436479]

Song J, Christian KM, Ming G-L, & Song H (2012). Modification of hippocampal circuitry by adult neurogenesis. Developmental Neurobiology, 72(7), 1032–1043. 10.1002/dneu.22014 [PubMed: 22354697]

Thaler JP, Yi C-X, Schur EA, Guyenet SJ, Hwang BH, Dietrich MO, … Schwartz MW (2012). Obesity is associated with hypothalamic injury in rodents and humans. The Journal of Clinical Investigation, 122(1), 153–162. 10.1172/JCI59660 [PubMed: 22201683]

Vaisse C, Halaas JL, Horvath CM, Darnell JE Jr., Stoffel M, & Friedman JM (1996). Leptin activation of Stat3 in the hypothalamus of wild-type and ob/ob mice but not db/db mice. Nature Genetics, 14 (1), 95–97. 10.1038/ng0996-95 [PubMed: 8782827]

Yasuo S, Yoshimura T, Ebihara S, & Korf H-W (2007). Temporal dynamics of type 2 deiodinase expression after melatonin injections in Syrian hamsters. Endocrinology, 148(9), 4385–4392. 10.1210/en.2007-0497 [PubMed: 17540726]

Yoo S, & Blackshaw S (2018). Regulation and function of neurogenesis in the adult mammalian hypothalamus. Progress in Neurobiology, 170, 53–66. 10.1016/j.pneurobio.2018.04.001 [PubMed: 29631023]

Yoo S, Cha D, Kim DW, Hoang TV, & Blackshaw S (2019). Tanycyte-independent control of hypothalamic leptin signaling. Frontiers in Neuroscience, 13, 240 10.3389/fnins.2019.00240 [PubMed: 30941008]

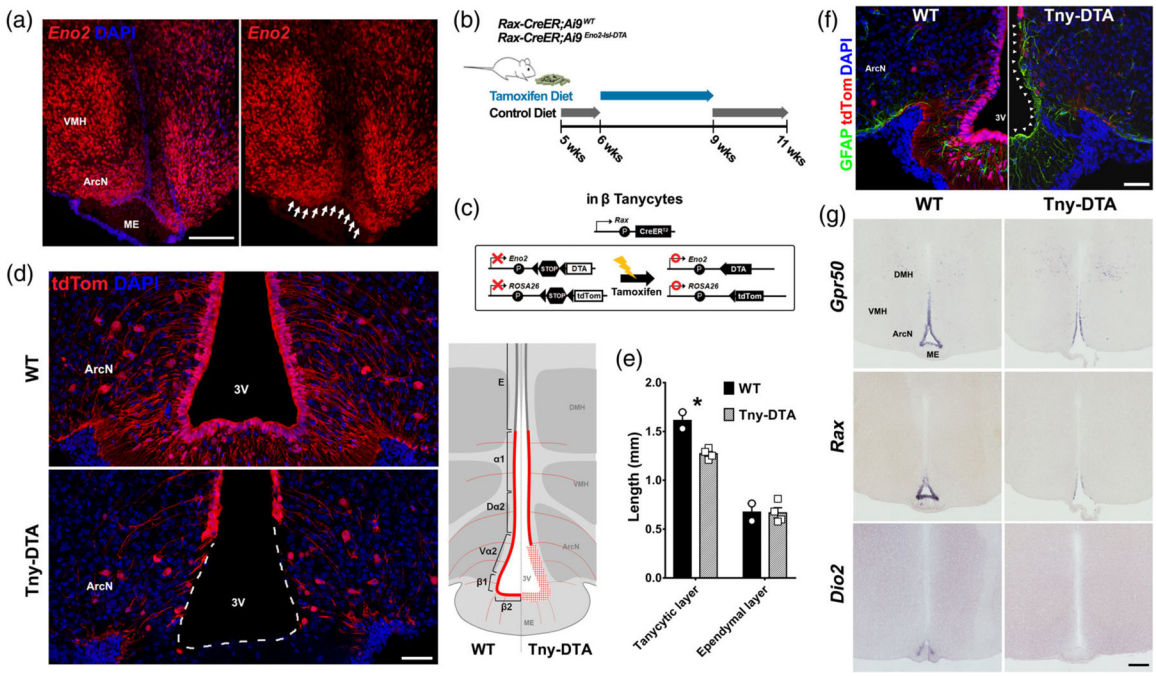

Figure 1.

Selective genetic ablation of tanycytes of the ArcN and ME. (a) *Eno2* mRNA expression in tanycytes located near the ArcN and ME (white arrows). (b) Schematic diagram showing the time schedule for administration of tamoxifen diet. Five-week-old *Rax-CreER;Ai9* (WT) or *Rax-CreER;Eno2-lsl-DTA;Ai9* (Tny-DTA) mice were fed with control diet which, aside from lacking tamoxifen, has the same dietary components as the tamoxifen diet, for a week followed by 3 weeks of tamoxifen diet. The mice had 1 week of washout to allow for clearance of tamoxifen before experiments were conducted. (c) Schematic diagram showing the approach used to conditionally ablate tanycytes of the ArcN and ME. By using the *Rax-CreER* line, *Cre* recombination induces *tdTom* expression in all subtypes of tanycyte while DTA expression is specific in Eno2-positive beta-tanycytes and ventral alpha-2 tanycytes. (d) Immunohistochemistry for tdTom showing nearly complete ablation of tanycytes in the ArcN and ME. A diagram inset on the right shows the ablated region (red plaid) lacking tdTom expression in the Tny-DTA mice. E, Ependymal cells; α1,alpha-1 tanycytes; Dα2, dorsal alpha-2 tanycytes; Vα2, ventral alpha-2 tanycytes; β1, beta-1 tanycytes; β2, beta-2 tanycytes. (e) Quantification of reduction of ventricular surface occupied with tdTom-positive tanycytes (tanycytic layer) following tamoxifen-induced ablation as shown in (d). Ependymal cells are indicated as tdTom-negative ventricular cells in the dorsal hypothalamus. (f) Immunohistochemistry for GFAP indicating glial scar formation in the ventricular region following tanycyte ablation (arrowheads). (g) mRNA in situ hybridization using probes for tanycyte marker genes *Gpr50*, *Rax*, and *Dio2*. There is no sex-difference in ablation pattern or scale, and only male data was used that correspond to the male-specific metabolic phenotype which will be shown later. Scale bar: 50 μm (d, f), 200 μm (a, g). *$p < .007$, two-tailed Student's *t* test

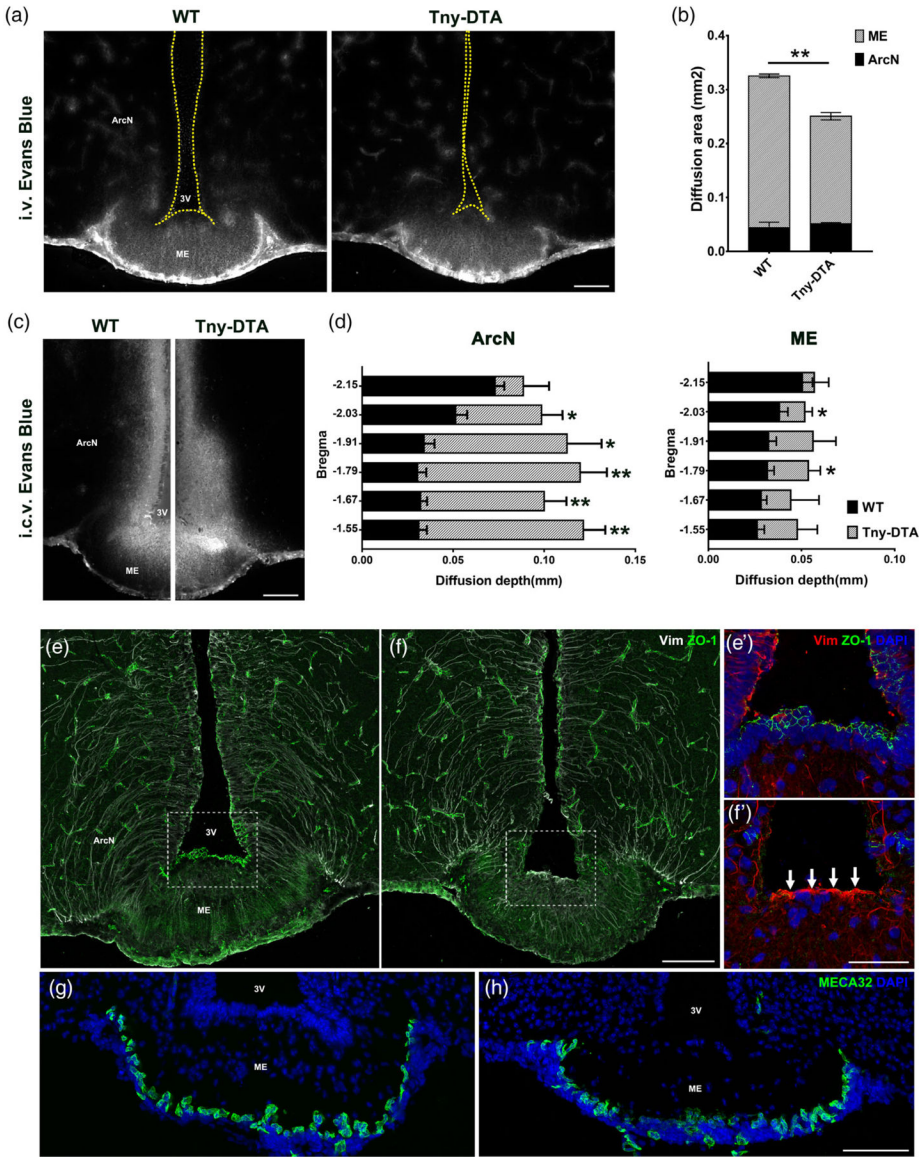

Figure 2.

Ventricular-hypothalamic barriers are disrupted in tanycyte-ablated mouse brain. (a) Representative images of Evans Blue staining in the ventromedial hypothalamus 20 min after i.v. injection. (b) Quantification of the area stained with Evans Blue shown (a), which is mostly restricted to the ArcN and ME. $n = 3$ per groups. (c) Representative images of Evans Blue staining 5 min after i.c.v. injection. (d) Quantification of the penetration of Evans Blue staining into the ArcN or ME shown (c) in the hypothalamic sections corresponding to the indicated bregma. $n = 3$ per groups. (e, f) Immunohistochemistry for the tight junction protein ZO-1 (green) and intermediate filament Vimentin (Vim, white). The staining patterns for ZO-1 and Vim were lost following tanycyte ablation. Increased Vim expression (white arrows) in the third ventricular floor reveals a glial scar formation. (e′, f′) are the higher magnification images of the boxed area in (e, f). (g, h) Immunostaining against the

fenestrated capillary marker, MECA32 (green). Scale bar: 100 μm (a, c, f, h), 50 μm (f′). *p < .05, **p < .005, two-tailed Student's t test

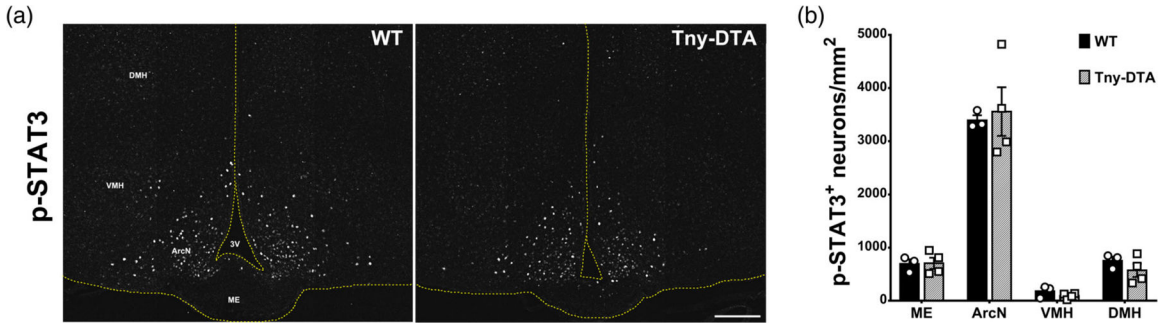

Figure 3.

Leptin-induced STAT3 phosphorylation in the hypothalamus of control and tanycyte-ablated mice. (a) Representative images of pSTAT3 immunohistochemistry 15 min after i.p. leptin injection. (b) Quantification of the pSTAT3-positive neurons in the images shown (a), $n = 3–4$. No significance found, two-way ANOVA followed by Sidak's multiple comparison. ArcN, arcuate nucleus; DMH, dorsomedial nucleus; ME, median eminence; VMH, ventromedial nucleus; 3 V, third ventricle. Scale bar: 100 μm (a) [Color figure can be viewed at wileyonlinelibrary.com]

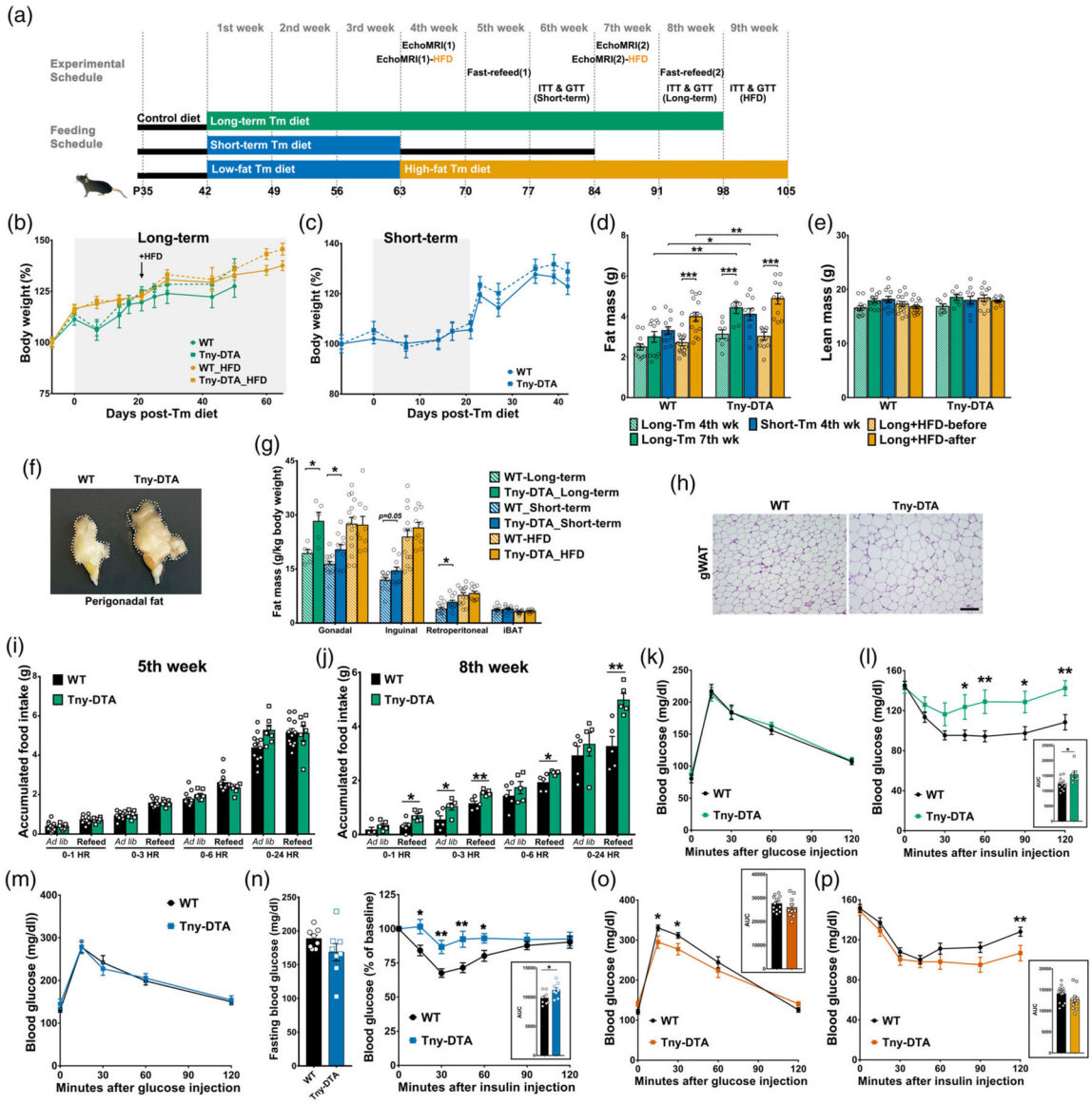

Figure 4.

Effect of tanycyte-ablation on body weight, fat mass, food intake, and glucose/insulin sensitivity. (a) Strategy for the long-term and short-term dietary tamoxifen administration and experimental schedule. (b) Body weight change during the long-term dietary tamoxifen administration based on either regular (green, n = 7–12 per group) or high-fat diets (HFD, orange, n = 10–12 per group). Gray background indicates the period of tamoxifen administration. The arrow indicates the time HFD was introduced. (c) Body weight change during the short-term dietary tamoxifen administration. Gray background indicates the period of tamoxifen administration. n = 11–15 per group. (d, e) Fat and lean mass measured by EchoMRI at 4 and 7 weeks following initiation of tamoxifen diet, or before and after high-fat tamoxifen diet (HFD). (f) A representative image of perigonadal fat pad of wildtype (WT) and tanycyte-ablated mice (Tny-DTA). (g) Weight of dissected fat pads. iBAT, interscapular brown adipose tissue. (h) Representative H&E staining of gonadal white

adipose tissue (gWAT). (i, j) Ad libitum (Ad lib) or 18 hr fasting-induced (refeed) food intake at 5 weeks (i) and 8 weeks (j) following initiation of tamoxifen diet. (k) Glucose tolerance test in long-term tamoxifen fed mice. n = 7–12 per group. (l) Insulin tolerance test in long-term tamoxifen-fed mice and area under the curve (AUC). (m) Glucose tolerance test in short-term tamoxifen-fed mice. n = 8 per group. (n) A downward trend in 2 hr-fasting glucose baseline (left panel) and insulin tolerance test when normalized as % of baseline in short-term tamoxifen fed mice (right panel). Area under the curve (AUC) is shown in inset. (o) Glucose tolerance test in HFD tamoxifen-fed mice and area under the curve (AUC). (p) Insulin tolerance test in HFD tamoxifen fed mice and area under the curve (AUC). Scale bar: 100um (M). *p < .05, **p < .02, **p < .002, two-way ANOVA followed by Sidak's multiple comparison for (d, e), otherwise two-tailed Student's t test; n, as indicated for (d, e, i, j, l, n–p)

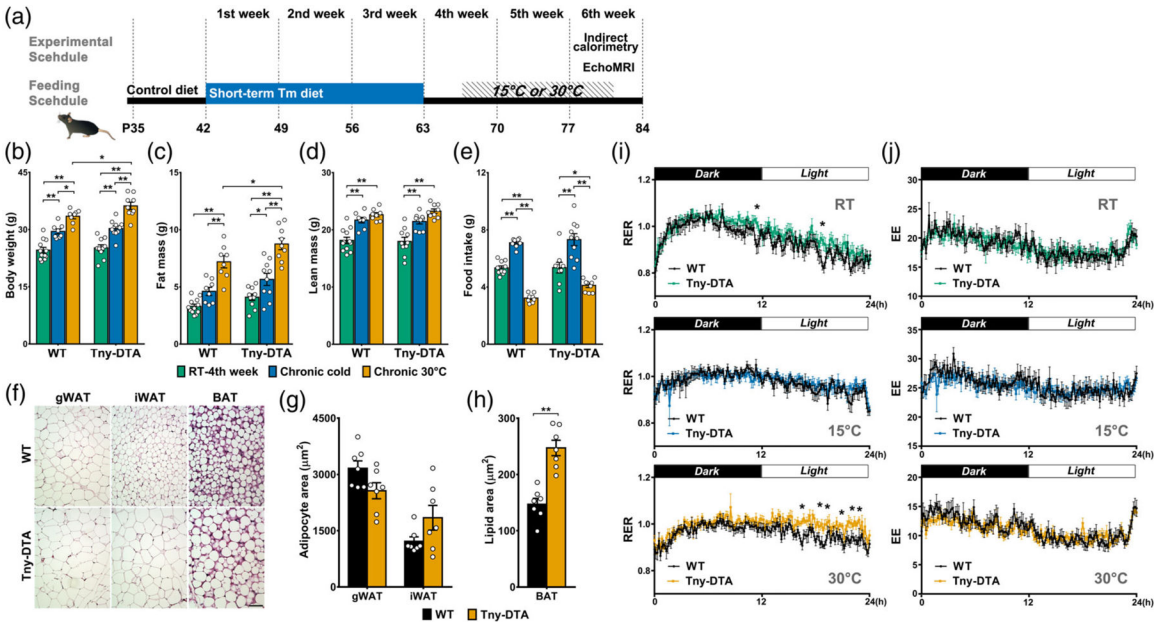

Figure 5.

Indirect calorimetry analysis of tanycyte-ablated mice at different housing temperatures. (a) Experimental schedule for indirect calorimetry after dietary tamoxifen administration. (b) Body weights of animals subjected to indirect calorimetry. (c, d) Fat and lean mass measured by EchoMRI at 4 weeks following initiation of tamoxifen diet or after 2 weeks of temperature change. (e) Food intake during metabolic profiling. (f) Representative images of fat pads of wildtype (WT) and tanycyte-ablated mice (Tny-DTA) at thermoneutrality. (g) Quantification of adipocyte size in gWAT and iWAT (f, left and middle panel, respectively), $n = 7$ per group. (h) Quantification of the lipid droplet size in BAT (f, right panel), $n = 7$ per group. (i) Respiratory exchange ratio (RER, VCO_2/VO_2) is measured at different temperature conditions. *, significant difference ($p < .05$, Student's t test) between groups analyzed for more than 30 min, $n = 8–10$ per group. (j) Energy expenditure (EE, kcal/kg/hr), measured along with RER(I) at different temperature conditions, $n = 8–10$ per group. BAT, brown adipose tissue; gWAT, gonadal white adipose tissue; iWAT, inguinal white adipose tissue. *$p < .04$, **$p < .001$, two-way ANOVA with Sidak's multiple comparison test; n, as indicated for (b–e)